Supporting Information

Nucleation, Coalescence, and Thin Film Growth of Triflate-Based Ionic Liquids on ITO, Ag, and Au Surfaces

Mariana S. M. Teixeira, Luís M. N. B. F. Santos, and José C. S. Costa*

CIQUP, Institute of Molecular Sciences (IMS), Department of Chemistry and Biochemistry, Faculty of Science, University of Porto, Rua do Campo Alegre, P4169 007 Porto, Portugal
**E-mail: jose.costa@fc.up.pt*

Index

Figure S1. Schematic representation of the vapor deposition/vacuum thermal evaporation methodology. **S3**

Figure S2. Schematic representation of the ovens of the ThinFilmVD apparatus. **S3**

Figure S3. Schematic representation and images of the substrate support system. **S4**

Figure S4. Illustration of the mechanisms of nucleation and growth of ionic liquid films. **S4**

Figure S5. Morphology of the substrates (ITO/glass, Ag/ITO/glass, and Au/ITO/glass). **S5**

Figure S6. Micrographs acquired through high-resolution scanning electron microscopy of vapor-deposited [C_2C_1im][OTF] onto surfaces of indium tin oxide (ITO)/, silver (Ag)/ITO, and gold(Au)/ITO. **S6**

Figure S7. Micrographs acquired through high-resolution scanning electron microscopy of vapor-deposited [C_4C_1im][OTF] onto surfaces of indium tin oxide (ITO)/, silver (Ag)/ITO, and gold(Au)/ITO. **S7**

Figure S8. Micrographs acquired through high-resolution scanning electron microscopy of vapor-deposited [C_6C_1im][OTF] onto surfaces of indium tin oxide (ITO)/, silver (Ag)/ITO, and gold(Au)/ITO. **S8**

Figure S9. Micrographs acquired through high-resolution scanning electron microscopy of vapor-deposited [C_8C_1im][OTF] onto surfaces of indium tin oxide (ITO)/, silver (Ag)/ITO, and gold(Au)/ITO. **S9**

Figure S10. Micrographs acquired through high-resolution scanning electron microscopy of vapor-deposited [$C_{10}C_1$im][OTF] onto surfaces of indium tin oxide (ITO)/, silver (Ag)/ITO, and gold(Au)/ITO. **S10**

Figure S11. Droplet size distribution of vapor-deposited ionic liquids onto ITO/glass and Ag/ITO/glass surfaces. **S11**

Figure S12. Schematic representation of the number of ionic liquid microdroplets formed per mm^2 of surface area and the respective surface coverage of those microdroplets as a function of each ionic liquid in the [$C_nC_1$im][OTF] series. **S12**

Table S1. Experimental conditions for the physical vapor deposition of each ionic liquid. **S13**

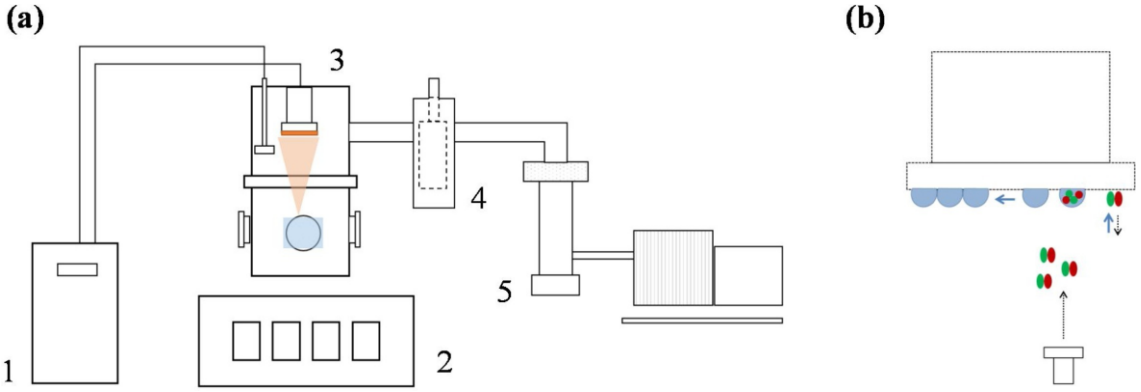

Figure S1. Schematic representation of the vapor deposition/vacuum thermal evaporation methodology: (a) ThinFilmVD apparatus (1 – cooling system, 2 – instrumentation box, 3 – vacuum chamber, 4 – N_2 (l) metallic trap, 5 – vacuum pumping system); (b) schematic detail of the PVD of ionic liquids by vacuum thermal evaporation from a Knudsen cell. More details: *Appl. Surf. Sci.*, 2018, 428, 242 and *J. Chem. Eng. Data*, 2015, 60, 3776.

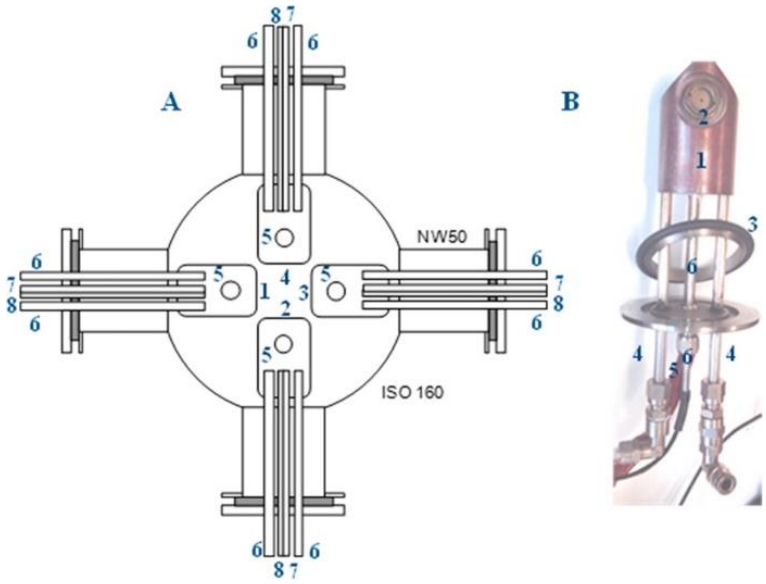

Figure S2. A – Schematic representation of the ovens of the ThinFilmVD apparatus: 1, 2, 3, 4 – individual copper ovens; 5 – cavity of the Knudsen cell screwing; 6 – air cooling tube; 7 – heater; 8, – Pt100 sensor; B – Image of an individual oven (top view): 1 – copper block; 2 – Knudsen cell; 3 – Viton O-ring; 4 – cooling system; 5 – heater; 6 – Pt100. More details: *J. Chem. Eng. Data*, 2015, 60, 3776.

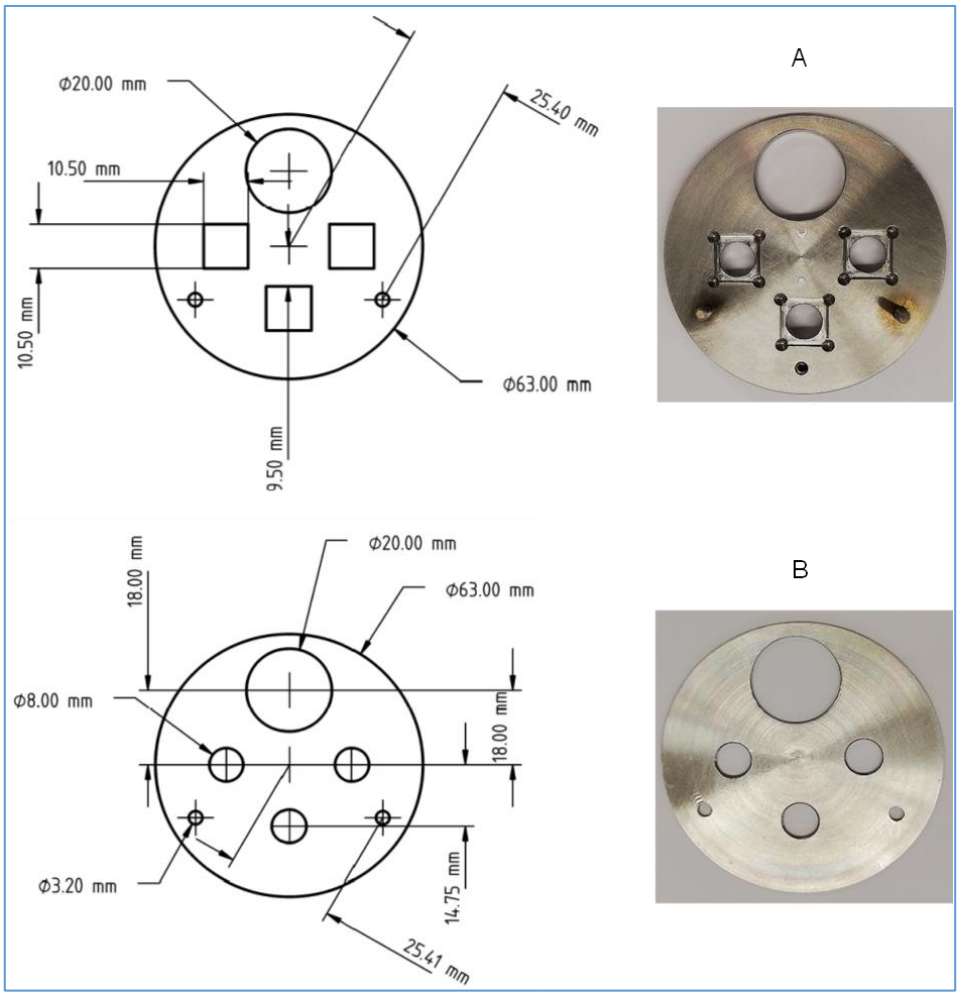

Figure S3. Schematic representation (left) and images (right) of the substrate support system. The support was used for the simultaneous deposition of each ionic liquid on three different surfaces: ITO/glass; Ag/ITO/glass; Au/ITO/glass.

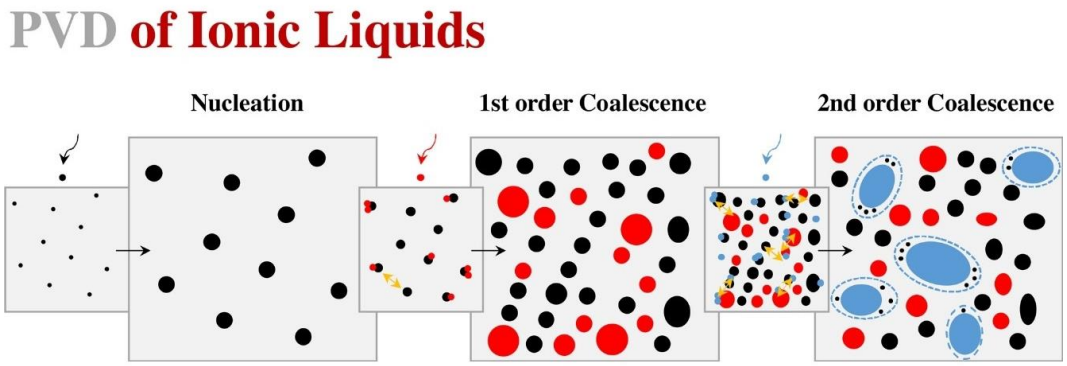

Figure S4. Illustration of the mechanisms of nucleation and growth of ionic liquid films: minimum free area to promote nucleation (MFAN); first-order coalescence; second-order coalescence. More details: *Appl. Surf. Sci.*, 2018, 428, 242.

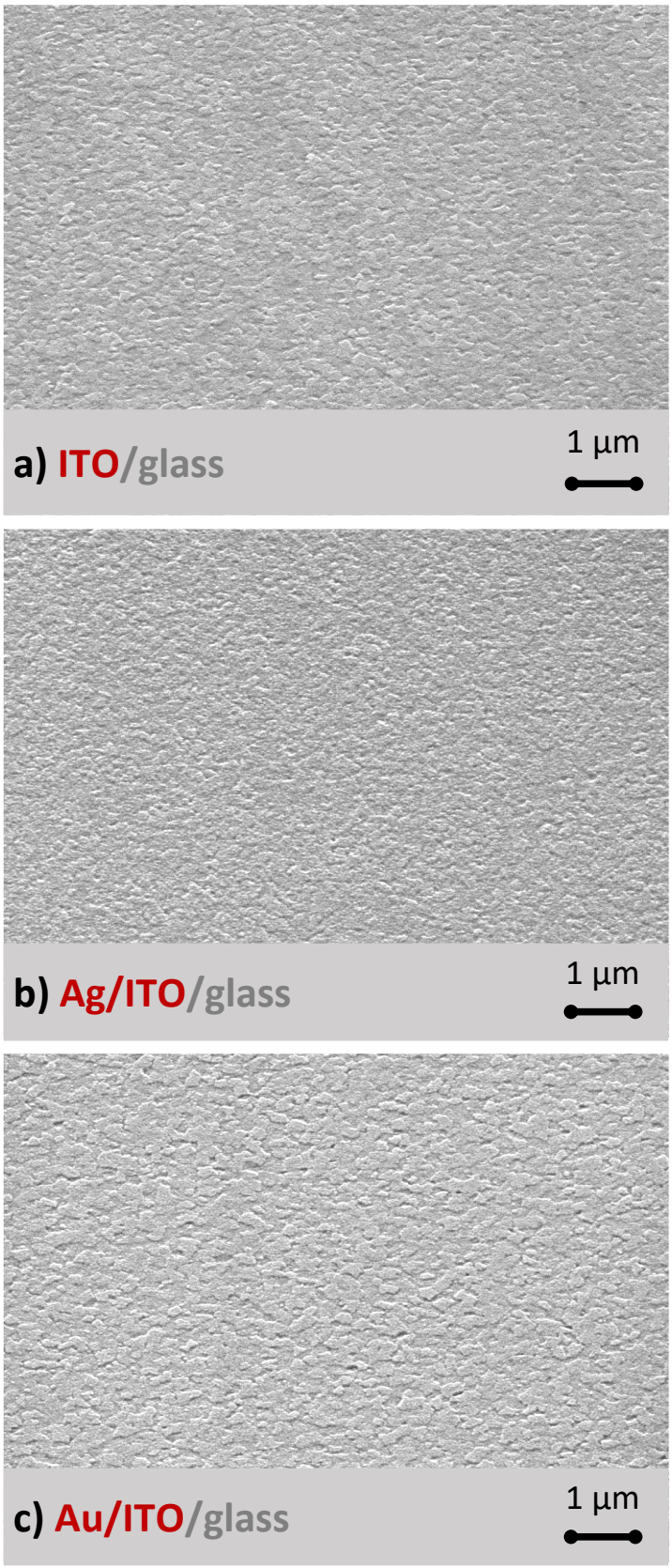

Figure S5. Morphology of the substrates: indium tin oxide (ITO)/glass surface (a); silver(Ag)/ITO/glass surface (b); gold(Au)/ITO/glass surface. Micrographs were acquired through high-resolution scanning electron microscopy (SEM) by using a secondary electron detector (SED). Lateral views at 45° were obtained with a magnification of 25000×.

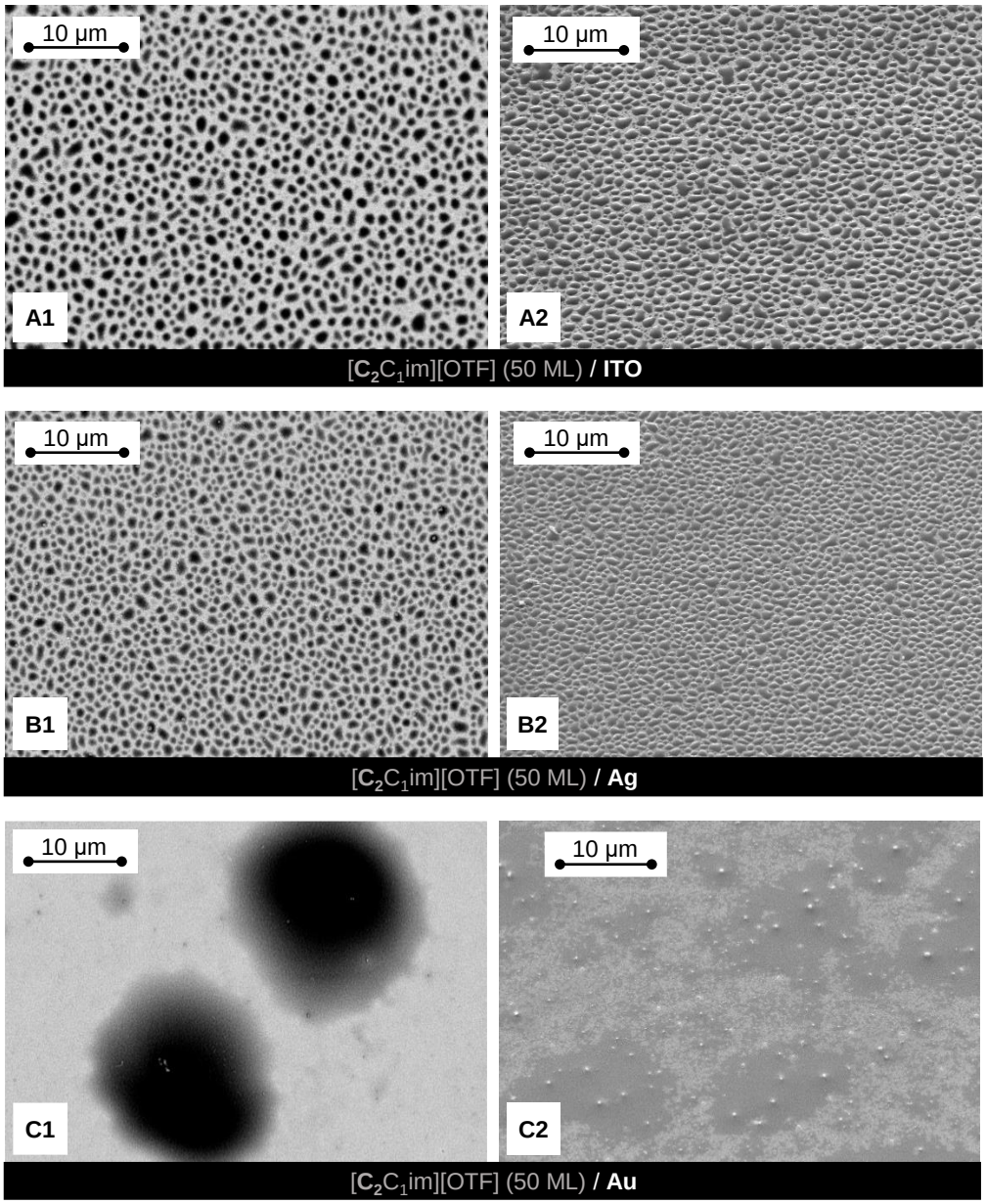

Figure S6. Micrographs acquired through high-resolution scanning electron microscopy of vapor-deposited [C_2C_1im][OTF] (50 monolayers, ML) onto surfaces of indium tin oxide (ITO)/glass (A1, A2), silver (Ag)/ITO (B1, B2), and gold(Au)/ITO (C1, C2). Top views (5000×) obtained by backscattered electron (A1, B1, C1) imaging, and lateral views at 45° (5000×) obtained by secondary electron imaging (A2, B2, C2).

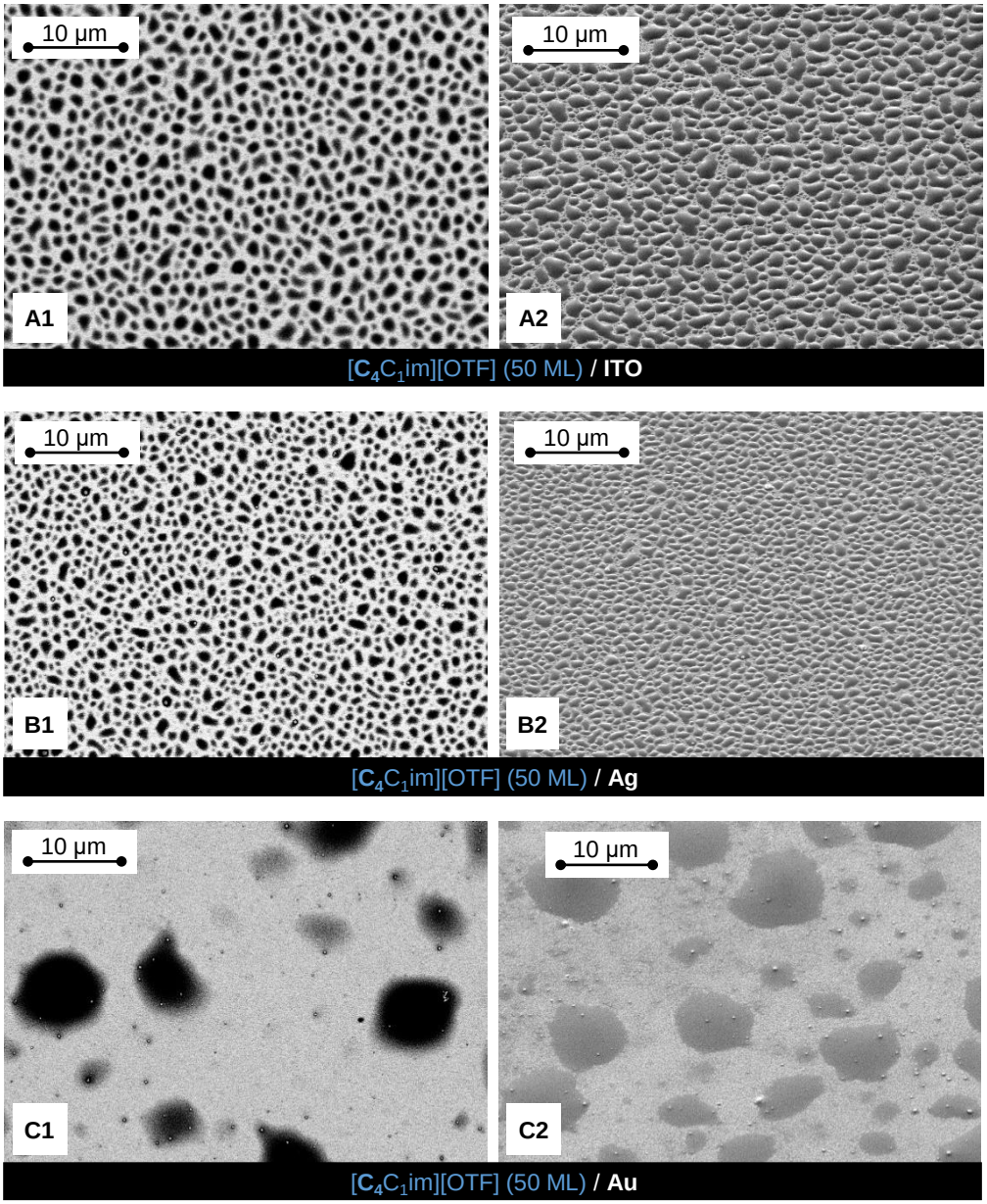

Figure S7. Micrographs acquired through high-resolution scanning electron microscopy of vapor-deposited [C_4C_1im][OTF] (50 monolayers, ML) onto surfaces of indium tin oxide (ITO)/glass (A1, A2), silver (Ag)/ITO (B1, B2), and gold(Au)/ITO (C1, C2). Top views (5000×) obtained by backscattered electron (A1, B1, C1) imaging, and lateral views at 45° (5000×) obtained by secondary electron imaging (A2, B2, C2).

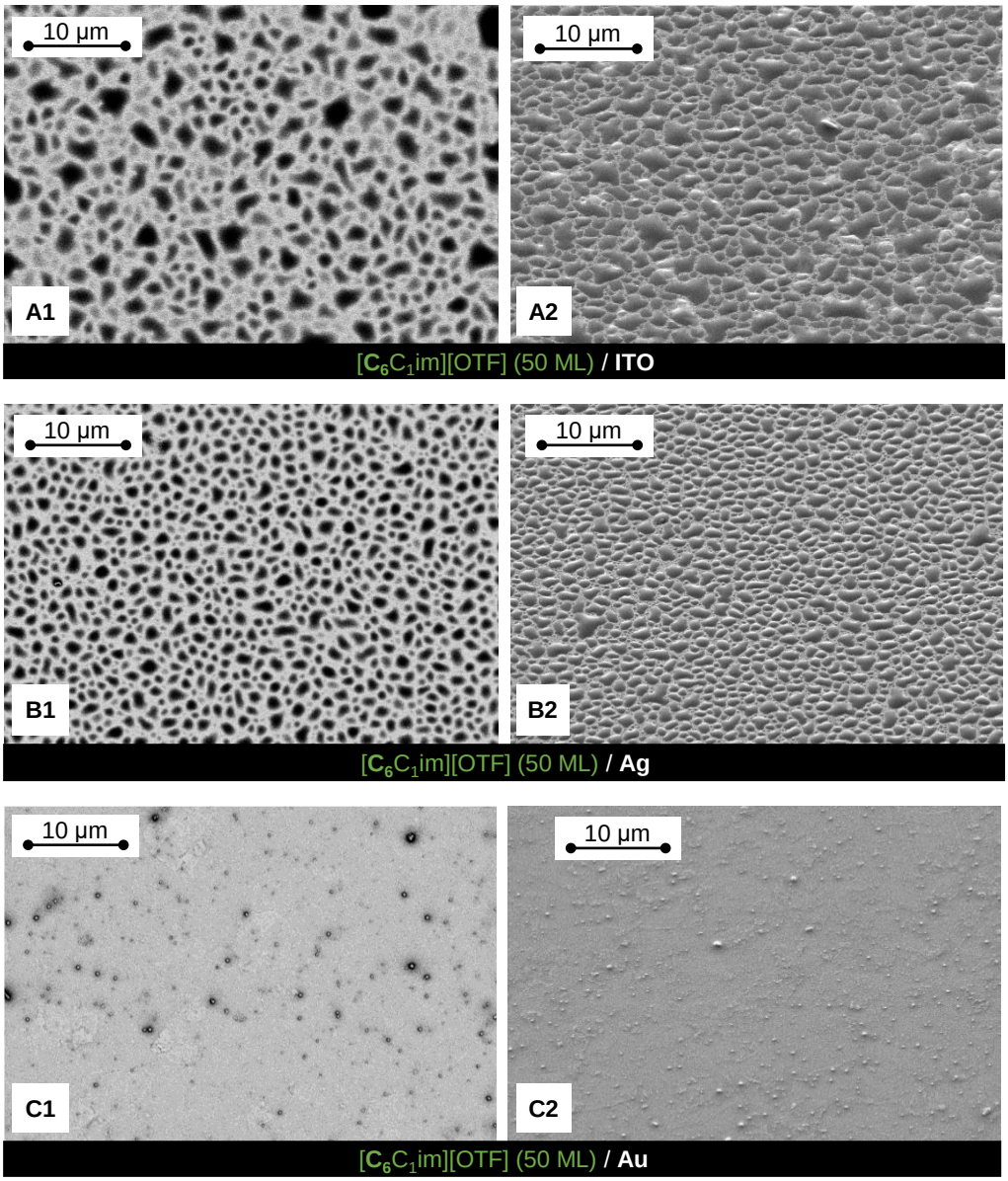

Figure S8. Micrographs acquired through high-resolution scanning electron microscopy of vapor-deposited [C_6C_1im][OTF] (50 monolayers, ML) onto surfaces of indium tin oxide (ITO)/glass (A1, A2), silver (Ag)/ITO (B1, B2), and gold(Au)/ITO (C1, C2). Top views (5000×) obtained by backscattered electron (A1, B1, C1) imaging, and lateral views at 45° (5000×) obtained by secondary electron imaging (A2, B2, C2).

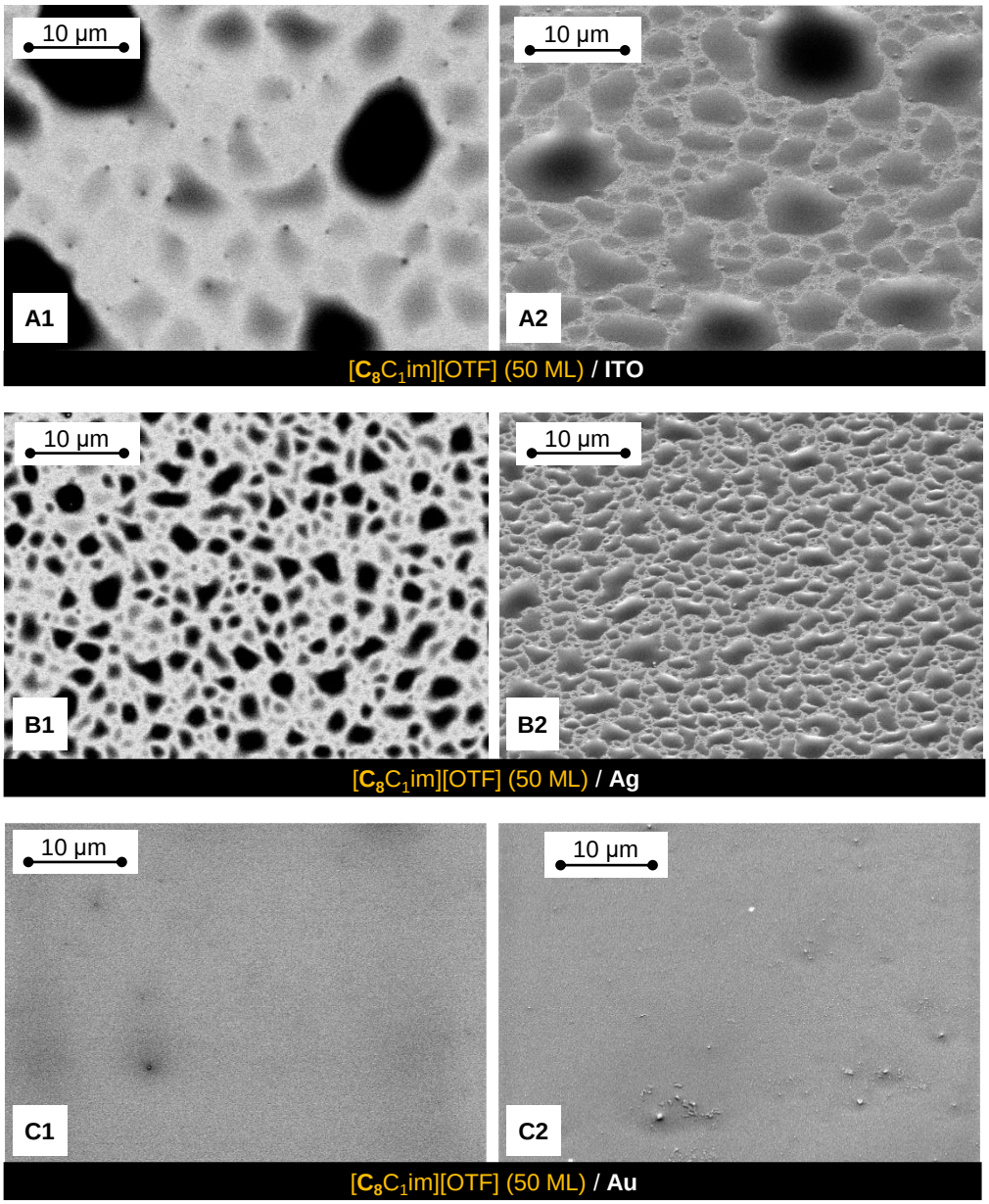

Figure S9. Micrographs acquired through high-resolution scanning electron microscopy of vapor-deposited [C_8C_1im][OTF] (50 monolayers, ML) onto surfaces of indium tin oxide (ITO)/glass (A1, A2), silver (Ag)/ITO (B1, B2), and gold(Au)/ITO (C1, C2). Top views (5000×) obtained by backscattered electron (A1, B1, C1) imaging, and lateral views at 45° (5000×) obtained by secondary electron imaging (A2, B2, C2).

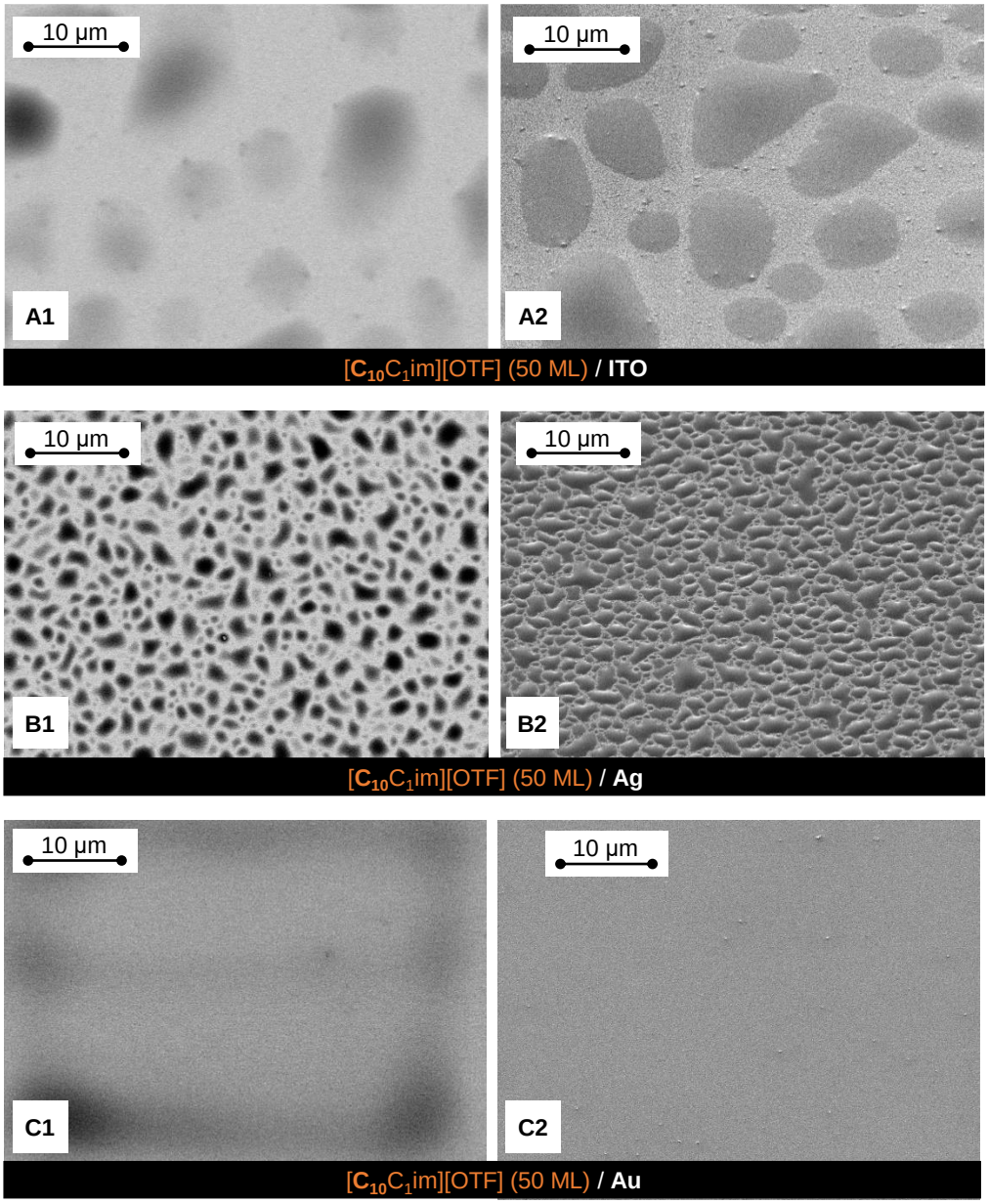

Figure S10. Micrographs acquired through high-resolution scanning electron microscopy of vapor-deposited [$C_{10}C_1$im][OTF] (50 monolayers, ML) onto surfaces of indium tin oxide (ITO)/glass (A1, A2), silver (Ag)/ITO (B1, B2), and gold(Au)/ITO (C1, C2). Top views (5000×) obtained by backscattered electron (A1, B1, C1) imaging, and lateral views at 45° (5000×) obtained by secondary electron imaging (A2, B2, C2).

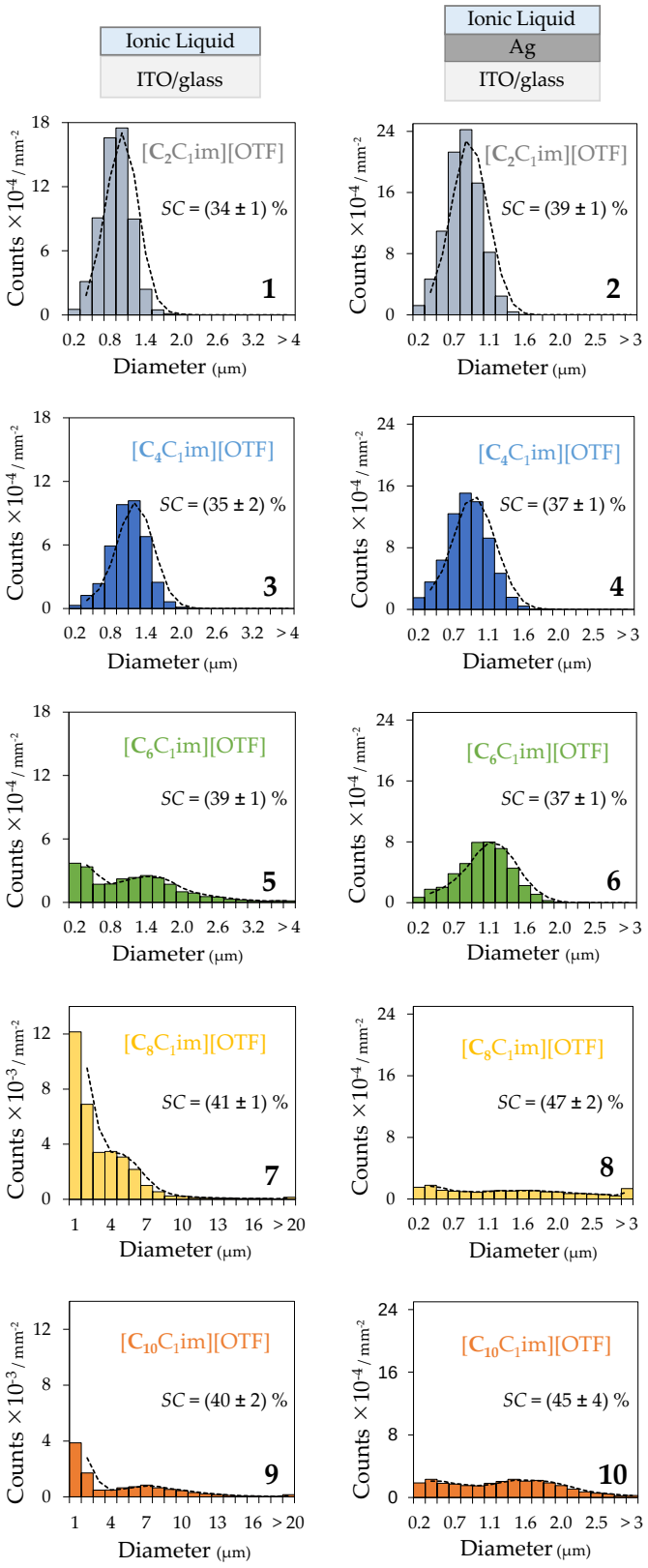

Figure S11. Droplet size distribution of vapor-deposited ionic liquids (50 monolayers, ML) onto ITO/glass (graphs on the left) and Ag/ITO/glass surfaces (graphs on the right): [C_2C_1im][OTF] (1,2); [C_4C_1im][OTF] (3,4); [C_6C_1im][OTF] (5,6); [C_8C_1im][OTF] (7,8); [$C_{10}C_1$im][OTF] (9,10). Values for the surface coverage (*SC*) are marked in each graph. The ionic liquids were deposited under the same experimental procedure and setup.

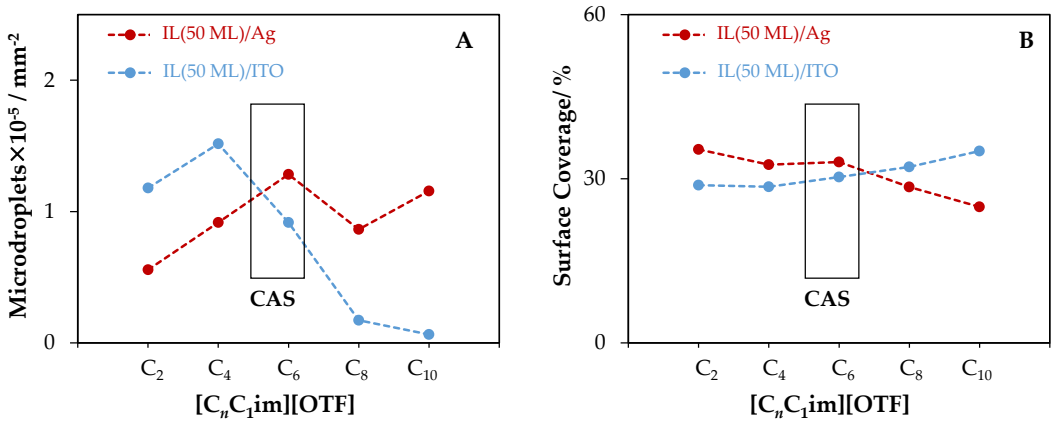

Figure S12. Schematic representation of the number of ionic liquid microdroplets (diameter above 1 μm) formed per mm^2 of surface area (graph A) and the respective surface coverage of those microdroplets (graph B) as a function of each ionic liquid in the [$C_nC_1$im][OTF] series.

Table S1. Experimental conditions for the physical vapor deposition/thermal evaporation of each ionic liquid: effusion temperature ($T_{eff.}$); equilibrium vapor pressure (*EVP*); mass flow rate at the Knudsen effusion cell orifice (Φ (Knudsen cell)); mass flow rate at the substrate surface (Φ (QCM)) and corresponding deposition rate in Å·s^{-1}; geometric factor; deposition time; thin film thickness (nm and ML).

Precursor	$T_{eff.}$	*EVP*	Φ (Knudsen cell)	Φ (QCM)	Geometric factor	Deposition rate	Deposition time	Thickness
	K	Pa	μg·cm^{-2}·s^{-1}	ng·cm^{-2}·s^{-1}		Å·s^{-1}	min	ML
[C$_n$C$_1$im][OTF] (50 ML) / substrate | substrates: Au/ITO; Ag/ITO; ITO								
[C$_2$C$_1$im][OTF]	513.2			4.4 ± 0.7		0.32 ± 0.05	≈ 18	
[C$_4$C$_1$im][OTF]	513.2			3.4 ± 0.7		0.26 ± 0.05	≈ 23	
[C$_6$C$_1$im][OTF]	513.2	≈ 0.1	≈ 30	4.1 ± 0.6	≈ 1×10^{-4}	0.33 ± 0.05	≈ 19	50
[C$_8$C$_1$im][OTF]	523.2			3.1 ± 0.6		0.26 ± 0.05	≈ 25	
[C$_{10}$C$_1$im][OTF]	523.2			3.5 ± 0.6		0.30 ± 0.05	≈ 23	